Archives of Environmental Protection
Vol. 51 no. 4 pp. 127–143

PL ISSN 2083-4772
DOI: 10.24425/aep.2025.157234

Trivalent antimony mineralization: Mechanism and application of *Acinetobacter johnsonii*

Xianrong Shi[1], Wanping Bian[2], Linping Yang[1], Jiuqin Xian[1], Kun Liu[1], Qian Wang[1], Aijiang Yang[1], Aping Niu*[1], Shixue Mei[1]

[1]Guizhou University, College of Resources and Environmental Engineering, Guizhou Karst Environmental Ecosystems Observation and Research Station, Ministry of Education, Key Laboratory of Karst Georesources and Environment, Ministry of Education, Guizhou University, Guiyang 550025, China
[2]Key Laboratory of Reservoir Aquatic Environment, Chongqing Institute of Green and Intelligent Technology, Chinese Academy of Sciences, Chongqing, 400714, China.

* Corresponding author's e-mail: apniu@gzu.edu.cn

Keywords: *Acinetobacter johnsonii*; Sb(III) biomineralization; EPS proteins; phytoremediation

Abstract. Current research on microbially mediated Sb(III) biomineralization has mainly focused on the role of polysaccharides in extracellular polymeric substances (EPS). In this study, we systematically investigated and confirmed the dominant regulatory role of protein components in EPS during Sb(III) biomineralization, thereby overturning the previous assumption that EPS polysaccharides are the primary functional component. A highly Sb-resistant strain, *Acinetobacter johnsonii*, was isolated. This strain exhibits remarkable characteristics: it can tolerate up to 21 mM Sb(III) stress, directionally mineralize Sb(III) into octahedral Sb_2O_3 microcrystals, and achieve a removal rate of up to 90% for 11 mM Sb(III). These results demonstrate its high Sb resistance and efficient, directional biomineralization capability. SDS-polyacrylamide gel electrophoresis (SDS-PAGE) and proteomic analysis confirmed that extracellular proteins (e.g. 34 kDa and 20 kDa) were upregulated under Sb(III) stress. Combined with EPS inactivation experiments, these results revealed the regulatory role of proteins: linearized peptide chains provide additional binding sites for Sb(III), promoting the formation of larger Sb_2O_3 microcrystals. This study thus clarifies the specific molecular mechanism underlying protein-mediated Sb(III) biomineralization. Furthermore, by integrating the microbial biomineralization mechanism with phytoremediation, a synergistic effect of "Sb immobilization and growth promotion" was achieved. This not only significantly reduced Sb accumulation in various rice tissues (roots, leaves, polished grains, and stalks) but also increaseds plant height and stabilized yield under Sb(III) stress. Our findings provide a novel application model of "pollution control and crop protection" for the remediation of Sb-contaminated farmlands.

Introduction

Antimony (Sb) is an environmental priority pollutant with metalloid properties. Industrial emissions and transportation-related activities (such as metallurgical slag heaps, electronic waste disposal, and brake pad wear) release large quantities of Sb-containing waste into soils and water bodies (Jabłońska-Czapla et al. 2022; Jabłońska-Czapla et al. 2024; Si et al. 2024). In the environment, Sb mainly exists in the form of trivalent (Sb(III)) and pentavalent (Sb(V)) forms. Sb(V) is the dominant form under aerobic conditions, whereas Sb(III) prevails in anaerobic environments. Sb(III) is more toxic than Sb(V), but the two species can interconvert and form precipitates, leading to changes in Sb speciation. Therefore, the toxicity and bioavailability of Sb in the environment are highly dependent on environmental conditions (Jabłońska-Czapla et al. 2015).

Water management practices have been shown to significantly affect the speciation and migration of Sb (Wu et al. 2022). For example, alternate wetting and drying (AWD) can regulate valence-state transformations and bioavailability of Sb by altering soil redox potential (Eh), pH, and the dissolution-precipitation equilibria (Chen et al. 2024; Wu et al. 2022). Rice, as a major cereal crop, is prone to Sb(III) accumulation. In recent years, several rice-growing areas have experienced varying degrees of Sb contamination (Zhang et al. 2017). Because rice is typically cultivated under flooded conditions, Sb(V) is readily reduced to Sb(III), posing significant risks to both ecosystems and human health. Developing effective strategies to remediate Sb-contaminated farmland has therefore become an urgent challenge for sustainable rice cultivation.

Plants and microorganisms play crucial roles in the transformation and immobilization of Sb (Devi et al. 2021; He et

al. 2023). The remediation of heavy metal pollution in farmland soil is mainly achieved through the passivation of heavy metals by microorganisms, which can reduce their uptake by plants. Microorganisms participate in the biogeochemical cycling of Sb through multiple mechanisms, including adsorption, redox reactions, methylation, and biomineralization (He et al. 2024). Among these mechanisms, biomineralization has attracted widespread attention as an energy-efficient and environmentally friendly approach for metal immobilization and the remediation of heavy-metal-contaminated farmland (He et al. 2025). Previous studies have shown that certain microorganisms can regulate Sb speciation by secreting extracellular polymeric substances (EPS). For instance, *Rhodotorula mucilaginosa* has been shown to induce the transformation of Sb(III) into Sb_2O_3 microcrystals, achieving a removal efficiency of up to 70% for 22 mM Sb(III) (Shukla et al. 2019; Yang et al. 2024). However, the mechanisms underlying Sb mineralization by bacterial extracellular polymers have not yet been thoroughly investigated, limiting the practical application of microbial remediation strategies.

At present, several research gaps remain regarding the specific mechanisms of Sb(III) biomineralization mediated by bacterial extracellular polymers (Dong et al. 2022). These include: (1) How do key components in EPS (e.g., proteins and polysaccharides) synergistically regulate the nucleation and growth of Sb_2O_3 crystals? (2) Do the molecular mechanisms and interfacial processes of Sb(III) biomineralization exhibit strain specificity? (3) Can microbially mediated Sb(III) biomineralization be coupled with phytoremediation strategies to achieve dual functions of Sb immobilization and crop growth promotion ? In addition, most existing studies have focused on the reductive pathways of Sb(V), whereas research on the direct microbial pathways of Sb(III) biomineralization and their applications in plant-soil interaction systems remains limited. In this study, a highly efficient Sb(III)-mineralization strain, *Acinetobacter johnsonii*, was used as the research subject to systematically investigate its mechanisms of Sb(III) tolerance, removal, and biomineralization. The objectives of this study are as follows: (1) to elucidate the changes in EPS components of *A. johnsonii* under Sb stress and their key roles in the formation of Sb_2O_3 crystals; (2) to clarify the molecular mechanism of underlying Sb(III) biomineralization; and (3) to evaluate the dual effects of this strain in inhibiting Sb uptake and promoting crop growth in a rice cultivation system. This study is the first to systematically reveal the mineralization mechanism of EPS secreted by *A. johnsonii* and its application in the remediation of Sb-polluted rice fields. It provides a novel strategy that combines theoretical insight with practical potential for the microbial remediation of Sb-contaminated farmland.

Materials and methods

Identification and cultivation of A. johnsonii

The samples for screening *A. johnsonii* were obtained from the bottom sediments of Lengshuigou Reservoir in Dushan County, Guizhou Province (107.77°E; 25.82°N). The isolation experiment and strain identification were conducted as described in the previous studies (Yang et al. 2024). Analytical grade potassium antimony tartrate ($C_8H_4K_2O_{12}Sb_2{\cdot}3H_2O$) was purchased from Huaxia Chemical. The LB medium (Luria-Bertani broth) composed of tryptone (10 $g{\cdot}L^{-1}$), yeast extract (5 $g{\cdot}L^{-1}$), and sodium chloride (NaCl) (10 $g{\cdot}L^{-1}$), is a bacterial culture medium widely used in microbiology and molecular biology experiments. The LB medium and all glassware required for the experiments were steam-sterilized before use. All reagents used were analytically pure. Three parallel experiments were set up for each group.

DNA was extracted following the manufacturer's instructions for the Power DNA Isolation Kit. Bacterial cultures (3 mL of overnight culture) were centrifuged at 4,000×g for 10 minutes to pellet the cells. The supernatant was discarded, and the cell pellet was resuspended in 100 µL of BDL buffer. Subsequently, 10 µL of lysozyme was added to the suspension, followed by incubation at 37°C for 10 minutes to ensure efficient cell lysis. The final DNA concentration was adjusted to 200 ng/µL. Polymerase chain reaction (PCR) amplification of the 16S rDNA was performed using the forward primer 27F (5'-AGAGTTT-GATCCTGGCTCAG-3') and reverse primer 1492R (5'-GGTTACCTTGTTACGACTT-3'). The PCR cycling conditions were as follows: initial denaturation at 98°C for 10 seconds, 35 cycles of denaturation at 98°C for 10 seconds, annealing at 55°C for 8 seconds, and extension at 68°C for 2 seconds. PCR products were purified by ethanol precipitation and sequenced using an ABI 3730X DNA Analyzer via the Sanger method. Raw sequencing data were assembled and edited bidirectionally using DNAMAN software to ensure sequence accuracy. The final concatenated sequence was submitted to GenBank under accession number MN216254.1 and subjected to homology analysis using the Basic Local Alignment Search Tool (BLAST) on the NCBI database (blast.ncbi.nlm.nih.gov). Phylogenetic analysis was performed using the neighbor-joining method based on 16S rDNA sequences.

Minimum inhibitory concentration (MIC), colony morphology, Gram staining, and bacterial morphology were determined according to previously described methods (Yang et al. 2024). LB media containing gradient concentrations of Sb(III) (0-25 mM) were prepared. The target strain was inoculated into media of each concentration at the same inoculum size, followed by shaking cultivation at 30°C. During cultivation, the optical density at 600 nm (OD_{600}) was measured regularly to monitor bacterial growth. When the Sb(III) concentration was ≤21 mM, the strain exhibited a normal growth rate and morphology, with OD_{600} values consistent with the logarithmic growth phase. When the concentration exceeded 21 mM, the strain's growth was significantly inhibited, OD_{600} values decreased remarkably, and cell lysis was observed.

To examine the impact of temperature, pH, and Sb(III) concentration on the growth of *A. johnsonii* and the associated pH variations, experiments were conducted using a 2% inoculum of *A. johnsonii*. Samples containing Sb(III) concentrations (0, 11, 14, and 17 mM) were cultured at 150 rpm, 30°C, and pH 7. Cultures containing 11 mM Sb(III) and different initial pH values (5, 7, and 9) were maintained at 150 rpm and 30°C, while those with 11 mM Sb(III) and varying temperatures (20, 30, and 40°C) were incubated at 150 rpm and pH 7. Throughout the experiment, pH values and optical density at 600 nm (OD_{600}) were measured regularly using a

pH meter and a UV-vis spectrophotometer (model S1020, Shanghai Tianmei Scientific Instrument Co., Ltd.).

Removal and transformation of Sb(III) by A. johnsonii

A 2% inoculum of *A. johnsonii* was added to LB medium containing 11 mM Sb(III), while cultures without Sb(III) served as the control. The cultures were incubated at 30°C and 150 r/min for 5 days. Bacterial suspensions (5 mL) were collected and centrifuged at 4°C and 8,000 r/min for 10 minutes. The supernatants and bacterial pellets from Sb-induced and non-induced cultures were collected. The concentrations of Sb(III) and Sb(V) in the supernatant were determined using an atomic fluorescence spectrophotometer (AFS-9800, Shanghai). Sb(III) and Sb(V) concentrations were calculated according to methods established in previous studies by our group (Yang et al. 2024). The removal efficiency of Sb(III) was calculated using equations (1).

$$Re = \frac{C_0 - C_t}{C_0} \times 100\% \quad (1)$$

where Re represents the removal efficiency of Sb(III), C_0 (mg/L) is the initial Sb(III) concentration, and C_t (mg/L) is the Sb(III) concentration in the supernatant after t hours of incubation. All concentrations are expressed in milligrams per liter (mg/L).

The experimental procedure involved determining the initial Sb(III) concentration (C_0) prior to incubation. Samples were then incubated under varying conditions (temperature, concentration, and pH), and the Sb(III) concentration (C_t) was quantified post-incubation to assess concentration changes under different experimental parameters.

The adsorption and absorption of bacterial cells for Sb(III) were determined according to the methods described in previous studies (Yang et al. 2024). After 5 days of cultivation, the precipitates collected from the bottom of the Erlenmeyer flasks were characterized using scanning electron microscopy (SEM) (ZEISS Sigma 300, Germany), X-ray photoelectron spectroscopy (XPS), and X-ray diffraction (XRD) (Bruker D8 Advance, Germany).

Analysis of supernatant composition and characterization of the precipitate formed in the supernatants

After cultivating *A. johnsonii* for 5 days under conditions with and without 11 mM Sb induction, the supernatants were obtained by centrifugation at 8,000 r/min for 10 minutes at 4°C. Protein content in the supernatants was determined using the Coomassie Brilliant Blue method, which is based on the binding of proteins with Coomassie Brilliant Blue (Nanjing Jiancheng Reagent Kit) to form a blue complex measured at a wavelength of 595 nm. Polysaccharide content was quantified using the sulfuric acid-anthrone method, in which polysaccharides are dehydrated under strongly acidic conditions to produce furfural derivatives that react with anthrone to yield a green complex, with absorbance measured at 620 nm. The polysaccharide concentration was calculated from a calibration curve prepared using glucose standard solutions at varying concentrations. To further investigate the composition and characteristics of the supernatant, three-dimensional excitation-emission matrix (3D-EEM) fluorescence spectroscopy was performed to identify different types of dissolved organic matter (DOM) (Yuan et al. 2011).

The supernatants of *A. johnsonii* cultures incubated for 5 days, with and without Sb(III) induction, were collected. The supernatants were then supplemented with 11 mM Sb(III) and incubated at 15°C (to prevent the growth of any remaining bacteria) and 150 rpm for 5 days. Meanwhile, the pH of the supernatants from Sb-induced and non-induced cultures was adjusted to approximately 8.5-9.0 to examine the effects of pH on precipitation morphology. An LB culture without *A. johnsonii* was used as a control. The precipitates formed in the supernatants were characterized by SEM and XRD.

Extraction of extracellular polysaccharides and its effect on Sb(III) mineralization

The supernatants of Sb-induced and non-induced *A. johnsonii* cultures were mixed with three volumes of pre-cooled 95% ethanol and left overnight. The mixtures were then centrifuged at 10,000 r/min for 15 minutes, and the resulting precipitates were completely dissolved in distilled water. An equal volume of 10% trichloroacetic acid solution was added to the dissolved precipitates, and the mixtures were left overnight. After centrifugation at 10,000 r/min for 20 minutes, the protein-containing precipitates were discarded. The supernatants were then mixed with three volumes of 95% ethanol and kept at 4°C overnight. Following centrifugation at 10,000 r/min for 30 minutes, the precipitates were collected into dialysis bags and dialyzed against ultrapure water at 4°C for 2 days, with the water replaced every 4 hours. The dialyzed samples were then freeze-dried to obtain crude extracellular polysaccharides (Chen et al. 2011). The obtained extracellular polysaccharides were dissolved in LB with pH 7, and 11 mM Sb(III) was added to the solution. The mixtures were then incubated at 30°C and 150 r/min for 5 days, and the formation of precipitates was subsequently examined.

SDS-polyacrylamide gel electrophoresis and proteome analysis of A. johnsonii supernatant

Polyacrylamide gel electrophoresis (SDS-PAGE) was used for the preliminary detection of proteins in the supernatants of Sb-induced and non-induced *A. johnsonii* cultured for 5 days. Samples were ultrafiltered using a 10 KDa cutoff to remove small-molecule impurities. Supernatants (30 μL) were mixed with loading buffer, heated at 70°C for 10 minutes, and centrifuged. Electrophoresis was performed at 160 V using Tris-Glycine-SDS buffer. Gels were stained with Coomassie Brilliant Blue and decolorized to visualize protein bands.

Protein samples were analyzed using shotgun proteomics. Samples were reduced with 100 mM DTT at 95°C for 5 minutes, cooled, and alkylated with 100 mM IAM in the dark for 30 minutes. After washing with 8 M UA and 25 mM ABC, proteins were digested overnight with a protease. The resulting peptides were desalted and purified for LC-MS/MS analysis. Mass spectrometry data were searched against the UniProt/NCBI databases. Proteins were evaluated for significance using Fisher's exact test, and KEGG (Kyoto Encyclopedia of Genes and Genomes) pathway analyses were conducted to elucidate functions and regulatory networks, with P-values < 0.05 indicating significant enrichment.

Characterization of the precipitate formed in non-inactivated and inactivated-EPS

The supernatants of Sb-induced and non-induced *A. johnsonii* cultured for 5 days were boiled in a water bath for 1 hour to inactivate EPS and used as controls. 11 mM Sb(III) was added to both boiled and unboiled supernatants, and the mixtures were incubated at 15°C and 150 r/min for 5 days. After incubation, the precipitates from different supernatants were collected, freeze-dried, and characterized using SEM, XRD, XPS.

Effect of A. johnsonii on Sb uptake of paddy

The growth promotion and antimony (Sb) adsorption experiment was conducted using Zhongzheyou 8 paddy rice. Soil samples were air-dried and sieved through a 2 mm mesh for pretreatment. Key physicochemical properties were determined as follows: pH was measured using a glass electrode method (soil-to-water ratio 1:2.5); total Sb content was quantified via aqua regia digestion followed by atomic fluorescence spectrometry (AFS) according to the Modern Analytical Methods for Soil Elements (GB/T 22105.2-2008); organic matter content was analyzed by the potassium dichromate oxidation-external heating method; and alkaline hydrolyzable nitrogen, available phosphorus, and available potassium were determined using the diffusion absorption method, sodium bicarbonate extraction-molybdenum Sb anti-colorimetric method, and ammonium acetate extraction-flame photometry, respectively (Long et al. 2018).

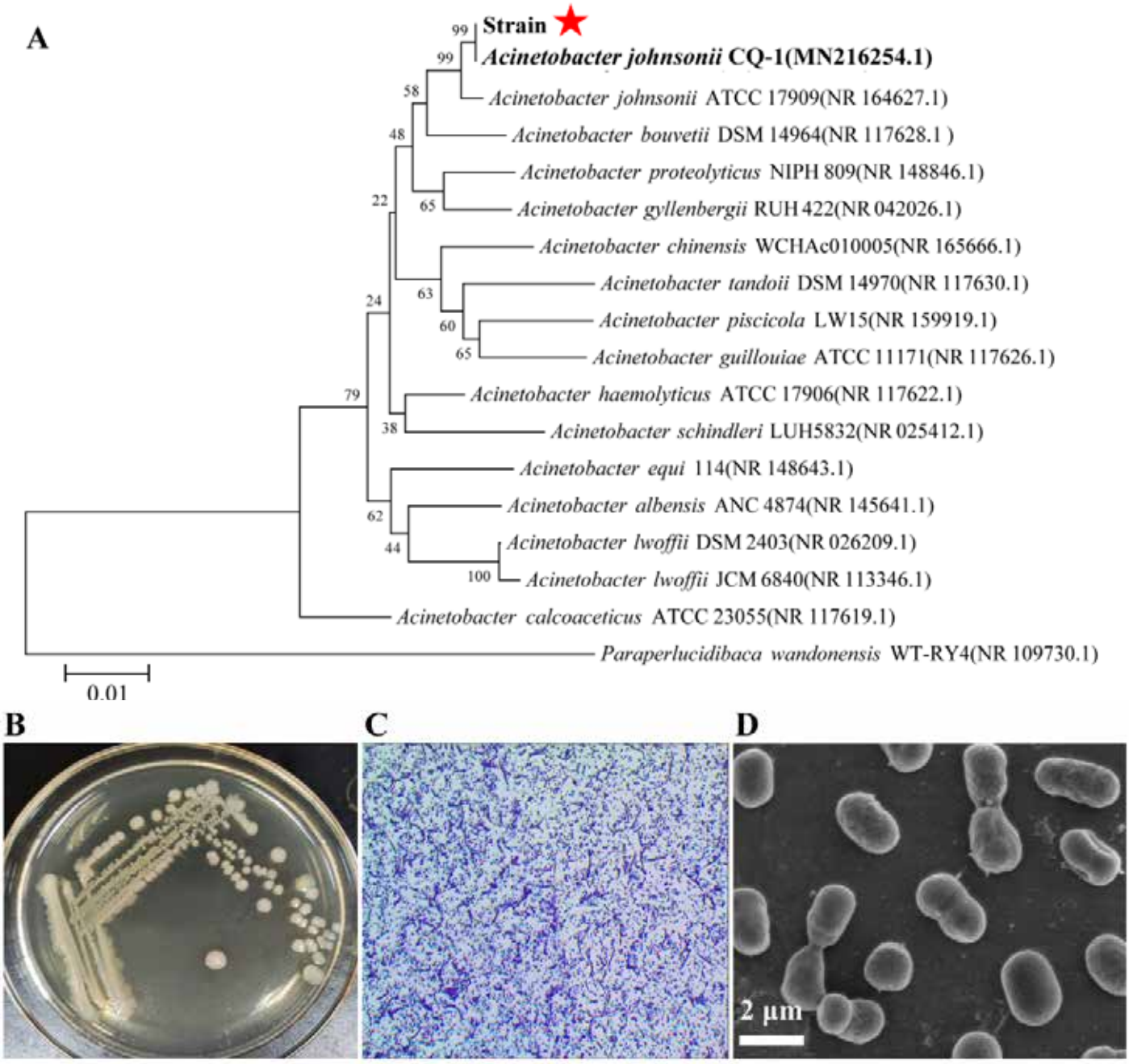

Fig. S1. Phylogenetic tree and morphology of A. *johnsonii*. (A) Phylogenetic tree showing the relationship of the microorganism with related bacteria; (B) Colonies of A. *johnsonii* on LB agar plates after 1 day of cultivation; (C) Gram staining and microscopic observation of colony morphology of A. *johnsonii* after 1 day of cultivation; (D) Scanning electron microscopy (SEM) observation of the cell morphology of A. *johnsonii* after 1 day of cultivation at 20×magnification.

Soil was spiked with Sb(III) at graded concentrations (10 , 50 , and 100 mg·kg^{-1}) and loaded into plastic pots (10 kg per pot), then equilibrated under natural conditions for 30 days to achieve phase distribution equilibrium. Five uniformly grown rice seedlings were transplanted into each pot. A 50 mL suspension of overnight-cultured *A. johnsonii* was inoculated into the rhizosphere, with non-inoculated treatments serving as controls. The saturated water level was maintained at 5 cm above the soil surface throughout the experiment. At maturity, rice yield and plant height were immediately recorded. Roots, stems, leaves, and polished grains were separated and oven-dried at 65°C to constant weight (approximately 2 days). All dried samples were pulverized, subjected to acid digestion, and analyzed for Sb concentrations using a dual-channel atomic fluorescence spectrometer (AFS-230E) (Long et al. 2018).

Statistical analysis

All experiments were performed in triplicate, and data were expressed as mean ± S.E.M using GraphPad Prism 10 software. The XPS peaks were fitted using XPSPEAK 4.1 software; while XPS, XRD, and 3D-EEM fluorescence spectra were plotted using Origin 2021. Statistical analyses were conducted using IBM SPSS Statistics 22.0 (SPSS Inc.USA). Differences between groups were assessed using two-way analysis of variance (ANOVA), with $p \leq 0.05$ considered statistically significant.

Results

Bacterial identification and growth metrics

A highly Sb-resistant microorganism was isolated from the bottom sediments of Lengshuigou Reservoir in Dushan County, Guizhou Province. This bacterium could tolerate up to 21 mM Sb(III). The target sequence of 1500 bp was successfully determined using Sanger sequencing (data are provided in the "Sanger sequencing data" file). The 16S rDNA sequence revealed 100% similarity between the screened bacterium and *A. johnsonii* strain CQ-1 (MN216254.1), confirming that the strain belongs to *Acinetobacter johnsonii* (Fig. S1A). The colony of this strain was dark yellow and opaque (Fig. S1B). Gram staining showed that the cells appeared pink, indicating that it was Gram-positive bacterium (Fig. S1C). SEM showed that the bacterium has a rod-shaped morphology with a length of approximately 1-2 μm (Fig. S1D).

To investigate the effect of Sb(III) on the growth of *A. johnsonii*, four different concentrations (0, 11, 14, and 17 mM) were selected based on MIC of 21 mM. Bacterial growth was monitored using OD_{600} values. The growth curves at different Sb(III) concentrations showed that *A. johnsonii* could grow under high Sb(III) stress (Fig. S2A), indicating a certain level of Sb(III resistance. To further characterize the strain, the pH of the culture was measured over time (Fig. S2B). The result showed that pH increased with incubation time and finally stabilized at 8.6 under different Sb(III) stresses, demonstrating that the strain possesses alkalinity-producing ability.

Based on the growth and pH changes of *A. johnsonii* at different Sb(III) concentrations, 11 mM Sb(III) was selected for further experiments. To further study the adaptability of *A. johnsonii* to different temperatures and pH levels, the strain was cultured at 20, 30, 40°C, and at initial pH values of 5, 7, and 9) (Fig. S2C). The results showed that *A. johnsonii* could grow at 20 and 30°C but not at 40°C, indicating that high temperatures inhibit its growth. Growth and pH measurements under different initial pH conditions showed that growth of *A. johnsonii* was consistent and that the culture pH gradually

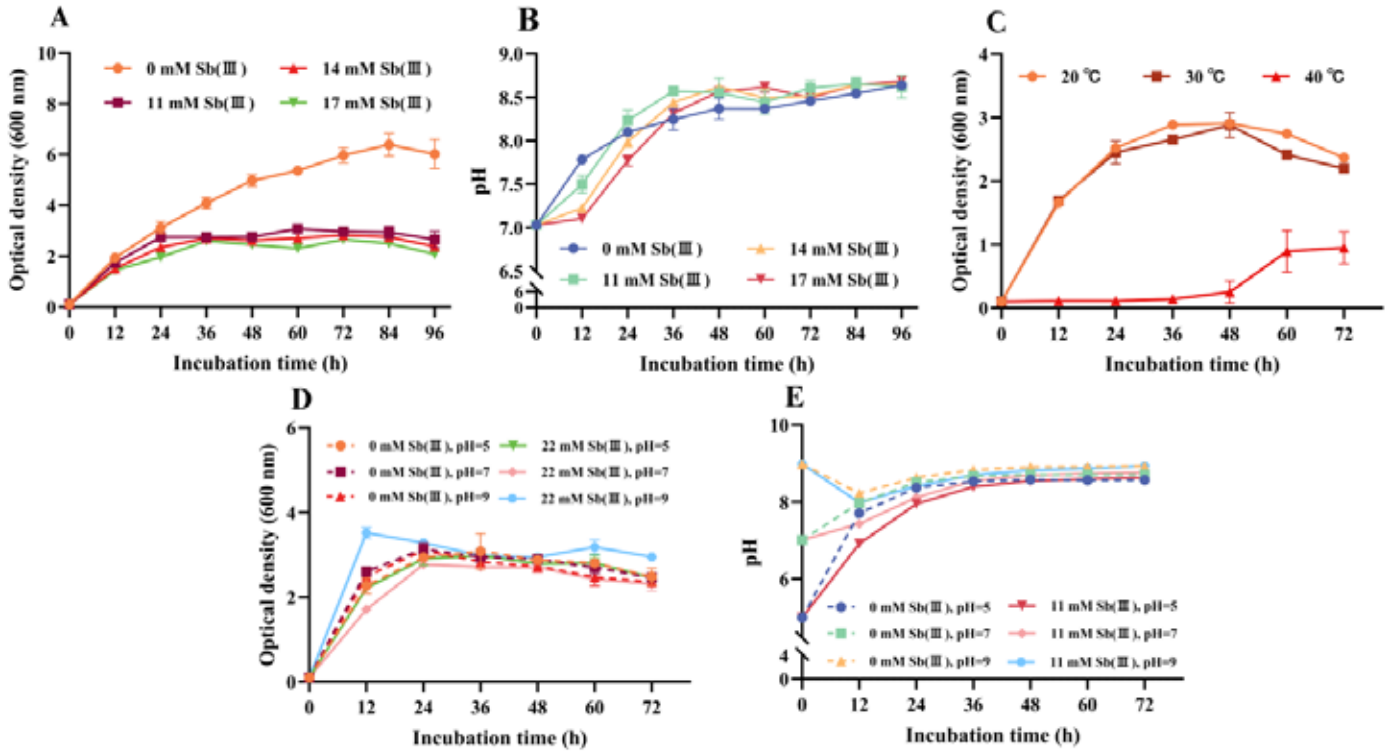

Fig. S2. Growth and pH changes of *A. johnsonii* under different conditions. (A) Growth curves and (B) pH changes at different concentrations of Sb(III); (C) Growth curves at different temperatures; (D) Growth curves and (E) pH changes at different pH values. Values are presented as the mean ± standard deviation (SD) of three replicate measurements (n = 3).

approaches 9 (Fig. S2D-E), indicating that pH did not affect the growth and alkalinity-producing capacity of *A. johnsonii*. Based on these results, 11 mM Sb(III), 30°C and pH 7 were selected for subsequent experiments to investigate the Sb(III) removal efficiency of *A. johnsonii*.

Removal and transformation of Sb(III) by A. johnsonii

To investigate the removal mechanism of *A. johnsonii* for Sb(III), the valence states Sb were first analyzed. The results showed a significant decrease of Sb(III) concentration accompanied by the formation of white precipitate in *A. johnsonii* culture. In contrast, no significant changes in Sb(III) concentration or white precipitate formation were observed in LB medium without *A. johnsonii* (Fig. 1A). Small amounts of Sb(V) were detected in both the treatment and control groups; however, the decrease in Sb(III) concentration was not proportional to the increase in Sb(V) concentration (Fig. 1A-B).

To further investigate the removal mechanism, the adsorption and absorption of Sb(III) by *A. johnsonii* were examined. The results indicated that the strain exhibited low adsorption and absorption efficiencies for Sb (Fig. 1C), suggesting that Sb(III) removal was primarily achieved through the formation of precipitate. The removal efficiency of *A. johnsonii* for Sb(III) was calculated using Eq. (1). The removal efficiency reached 80% on the first day and eventually stabilized at 90% by the 5th day, indicating a high Sb(III) removal capacity of the strain (Fig. 1D).

The white precipitate produced by *A. johnsonii* was characterized using SEM, XPS, and XRD. SEM showed that the precipitate formed in the culture of *A. johnsonii* exhibited an octahedral shape with a glazed surface and incomplete apex, with a size of 3.5 μm (Fig. 2A). XPS analysis indicated the presence of only Sb(III) at the binding energies of Sb $3d_{3/2}$ and Sb $3d_{5/2}$, confirming that the precipitate was composed of Sb(III) (Fig. 2C,D). XRD analysis showed that the diffraction

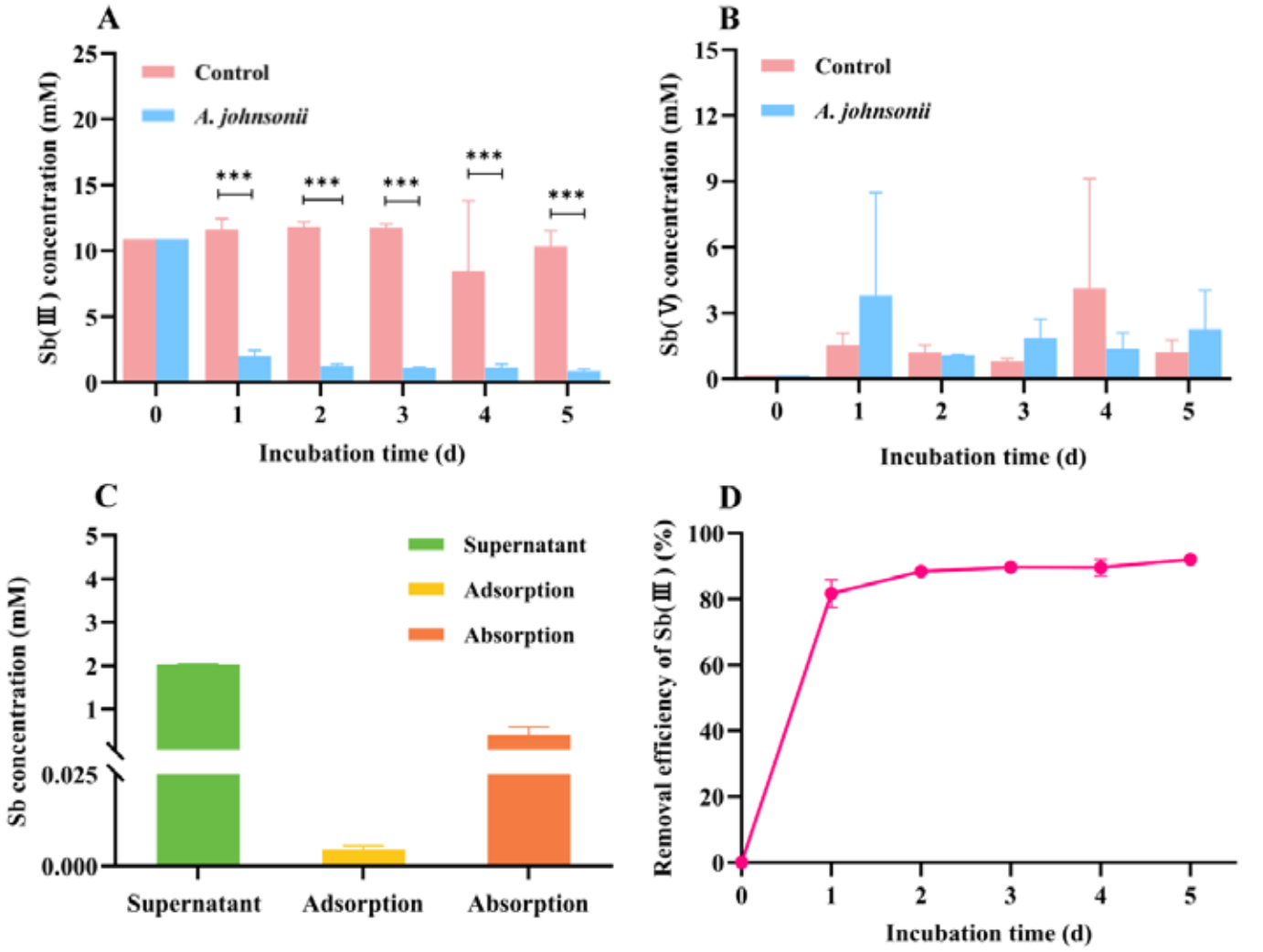

Fig. 1. The concentration of Sb in different valence states and Sb removal efficiency. (A, B) Changes in Sb(III) and Sb(V) concentrations in the culture medium; (C) Total Sb concentration in the supernatant, adsorption and absorption by cells induced by 11 mM Sb(III) for 5 days; (D) Removal efficiency of 11 mM Sb(III) by *A. johnsonii*. Differences between groups were analyzed using two-way analysis of variance, with $p \leq 0.05$ as significant differences.

In this figure, "***" indicates that there is an extremely significant statistical difference ($P < 0.001$) in the Sb(III) concentration between the group with *A. johnsonii* and the control group at the corresponding incubation time. This suggests that the presence of *A. johnsonii* has a very pronounced and highly significant effect on reducing the concentration of Sb(III) compared to the control condition without the bacterium.

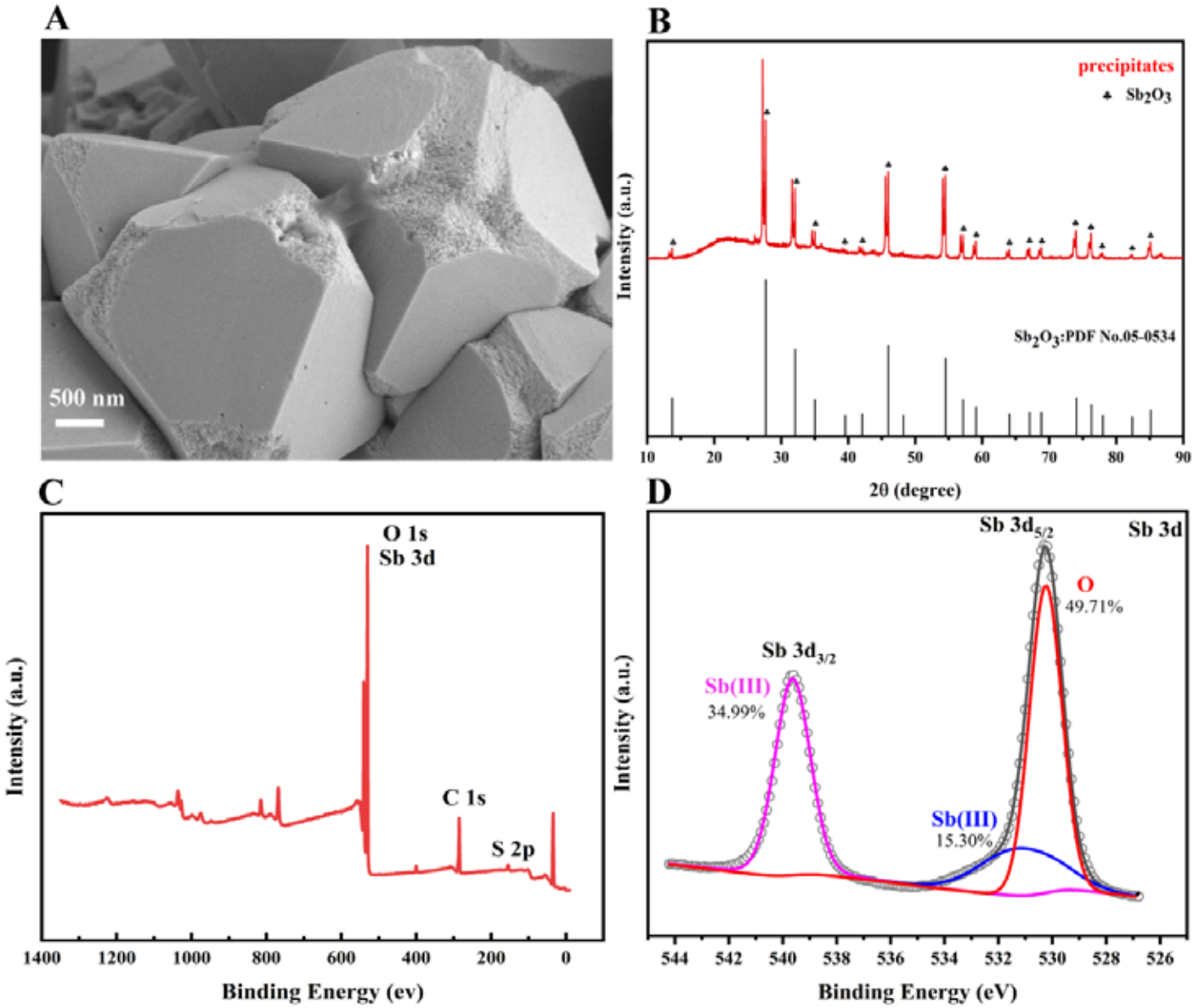

Fig. 2. Characterization and analysis of precipitates. (A) Scanning electron microscope (SEM); (B) X-ray diffraction (XRD); (C-D) X-ray photoelectron spectroscopy (XPS).

peaks of the precipitate matched those of the standard PDF card for Sb_2O_3 (PDF No. 05-0534), confirming its identity as Sb_2O_3 (Fig. 2B). Together, XRD and XPS analyses verified that the precipitate generated by *A. johnsonii* was Sb_2O_3.

Characterization of the precipitate formed in the supernatants

To further investigate the removal mechanism of *A. johnsonii* for Sb(III), the effects of different supernatants on Sb(III) transformation were examined. Sediments were observed in the supernatants of both Sb-induced and non-induced *A. johnsonii*, with or without pH adjustment. SEM revealed that the precipitates formed in the Sb-induced and non-induced supernatants exhibited distinct morphologies and sizes. In the non-induced supernatant, irregular, loose particles 1 μm in size were formed, whereas in the induced supernatant, dense octahedral granules with smooth surfaces were observed, with a slightly larger size of 1.2 μm, indicating that the Sb-induced supernatant plays an important role in controlling precipitate morphology. To assess the pH effects on Sb(III) mineralization, the pH of both supernatants was adjusteed to approximately 9 after adding Sb(III). SEM showed that the overall morphologies of the sediments remained unchanged in both pH-adjusted induced or non-induced supernatants, although the size of granules (1.2 μm) in the induced supernatant slightly decreased, suggesting that pH has a minor effect on granule morphology, while Sb-induced factors predominantly regulate the shape.

To further explore the impact of pH on Sb_2O_3 nucleation, LB culture with and without pH adjustment was used as controls. In LB medium, precipitate formed onlu in pH-adjusted LB (pH 8.5), and the particle size (0.8 μm) was smaller than those formed in the supernatants (Fig. S3A-C). XRD analysis showed that the main diffraction peaks of the precipitates generated in all supernatants corresponded to cubic-phase Sb_2O_3 (Fig. S3D), indicating that soluble Sb(III) was transformed into Sb_2O_3 in the supernatants of *A. johnsonii*. Overall, the characterization of precipitates confirmed that the

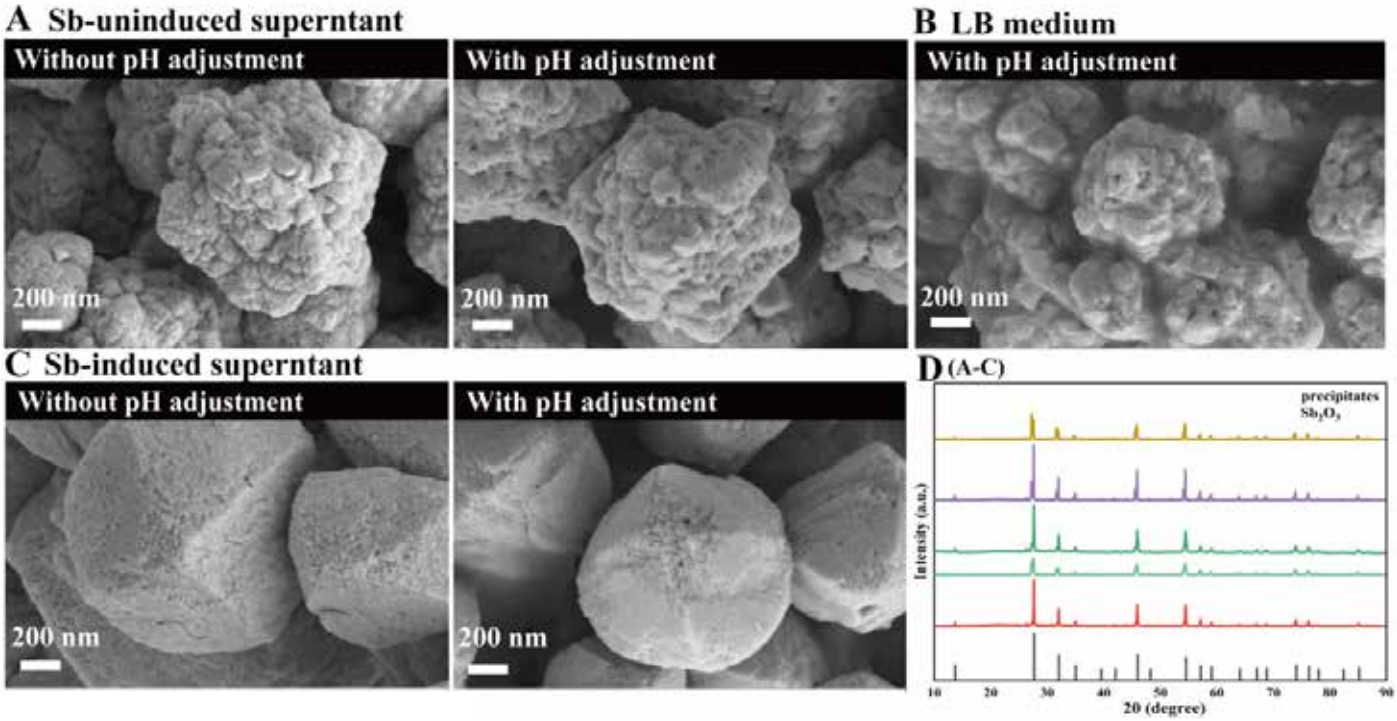

Fig. S3. Morphological changes and component analysis of precipitates formed from *A. johnsonii* supernatant during low-temperature mineralization process. (A) Sb-uninduced supernatant + 11 mM Sb(III): without pH adjustment; without pH adjustment; (B) LB +11 mM Sb(III): with pH adjustment; (C)Sb-induced supernatant + 11 mM Sb(III): without pH adjustment; without pH adjustment; (D) X-ray diffraction (XRD) corresponded to (A-C) in SEM;

supernatants of *A. johnsonii* can induce the formation of Sb_2O_3 and that the Sb-induced supernatant can regulate the formation of Sb_2O_3 with specific morphologies.

Microorganisms possess the ability to secrete polysaccharides and proteins, which play crucial roles in the biomineralization of heavy metals (Yu et al. 2022). Certain microbial-secreted proteins function as enzymes capable of catalyzing the redox reactions of heavy metals, thereby reducing the toxicity of Sb (Gaur et al. 2021). Meanwhile, microbial-produced polysaccharides can form complexes or precipitates with heavy metal ions, decreasing their bioavailability. Additionally, these abundant organic materials, such as proteins and polysaccharides, further facilitate the immobilization of Sb through microbially mediated organo-Sb complexation (Kondakindi et al. 2024). The contents of proteins and polysaccharides in the supernatant of *A. johnsonii*, with and without Sb(III) induction during incubation were measured. On the 5th day of cultivation, the concentrations of proteins and polysaccharides secreted by *A. johnsonii* in the absence of Sb(III) induction were approximately 60 mg/L and 3000 mg/L, respectively. Under Sb(III) induction, the concentration of secreted proteins remained at approximately 60 mg/L, whereas the concentration of polysaccharides decreased to about 2500 mg/L (Fig. S3G,H). The results showed that large amounts of polysaccharides and a certain amount of protein were secreted in both supernatants.

To further investigate the mineralization mechanism of *A. johnsonii* for Sb(III), polysaccharides were extracted from Sb-induced and non-induced supernatants, and their effects on Sb(III) mineralization were examined. No precipitates were generated in extracellular polysaccharides. Protein contents in the Sb(III)-induced supernatant were higher on day 1 compared to the non-induced supernatant, but reduced at intermediate period of cultivation. This suggests that Sb(III) induces the expression of specific proteins, which may bind Sb(III), leading to the reduction in protein content during incubation. The components of the supernatants were further analyzed by 3D-EEM fluorescence spectroscopy. Fluorescence peaks in both supernatants were situated in region IV, corresponding to soluble microbial byproducts, primarily tryptophan (Ex/Em 260/350 nm) and tyrosine (Ex/Em 275/305 nm) derivatives (Zhang et al. 2022) (Fig. S3E,F). Fluorescence intensity in the Sb(III)-induced supernatant was stronger on day 1 than in the non-induced supernatant, and decreased during at the intermediate period of cultivation, consistent with the observed changes in protein content.

SDS-PAGE and proteomic analysis of supernatants

In order to further investigate the role of extracellular proteins in Sb(III) mineralization, the protein expression profiles in Sb-induced and non-induced supernatants were analyzed. SDS-PAGE results showed that certain proteins were overexpressed at 34 kDa and 20 kDa in Sb-induced supernatant compared with the non-induced supernatant (Fig. 3A), indicating that Sb induction significantly altered the expression levels of these proteins. Proteomic analysis was subsequently performed to identify differential proteins. The results revealed that 30 differential proteins were significantly up-regulated in the Sb-induced supernatant compared to non-induced supernatant (Table S1), suggesting that these overexpressed proteins may play important roles in the mineralization of Sb(III). KEGG enrichment analysis showed that 10 of the upregulated proteins were involved in metabolic and degradation pathways (Fig. 3B).

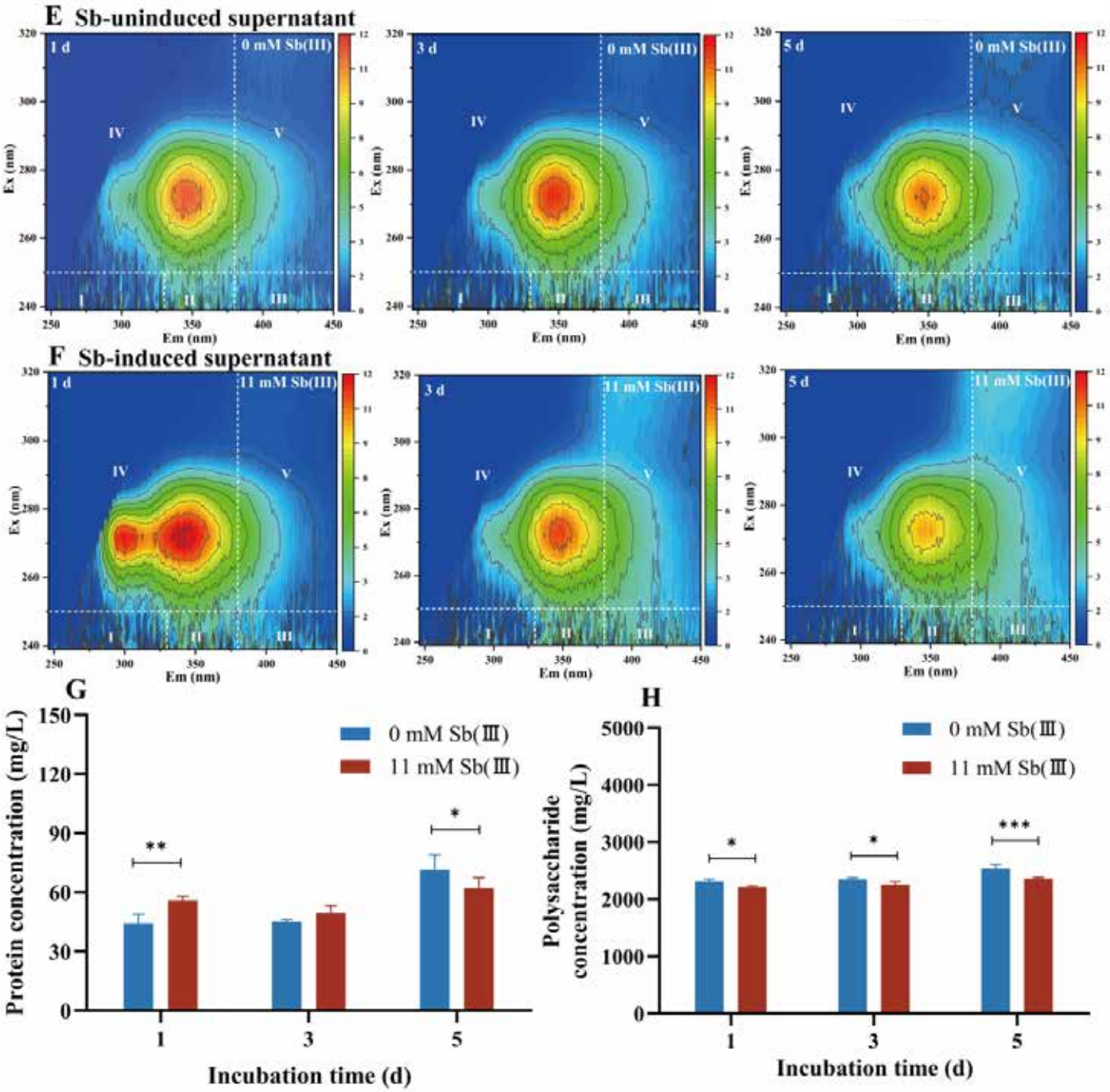

Fig. S3. Morphological changes and component analysis of precipitates formed from *A. johnsonii* supernatant during low-temperature mineralization process. (E-F) 3D-EEM spectroscopic analysis of supernatants of *A. johnsonii* cultured at 0 mM and 11 mM Sb(III) for 1, 3 and 5 days; (G) the changes in protein (TP) content; (H) polysaccharide content of *A. johnsonii* cultured for 1, 3, and 5 days under 0 mM and 11 mM Sb(III) conditions. Differences between groups were analyzed using two-way analysis of variance, with $p \leq 0.05$ as significant differences.

The effect of non-inactivated and inactivated EPS on Sb(III) mineralization

To further investigate the role of extracellular proteins on Sb(III) mineralization, deactivated supernatants were used to assess the effect of protein structure on Sb(III) mineralization. As depicted in Fig. 4A-B, the morphological changes and characteristics of precipitates formed by both Sb-induced and non-induced supernatants were examined during low-temperature mineralization to elucidate the mechanism of antimony mineralization. Precipitate formed in inactivated Sb-induced supernatant possesses incomplete octahedron shape with larger size comparing to corresponding non-inactivated supernatant. Precipitates formed in non-induced supernatants were both irregularly grainy, but the size of precipitates formed in inactivated supernatant was also larger than that formed in corresponding non-inactivated supernatant. This may be due to inactivated polypeptide chains providing additional binding sites for Sb(III) complexation, resulting in larger crystals. XRD analysis confirmed that the positions of the diffraction peaks in all samples matched the PDF card of Sb_2O_3 (Fig. S4A). XPS analysis indicated that only Sb(III), with binding energies corresponding to Sb $3d_{3/2}$ and Sb $3d_{5/2}$ was present in all precipitates. Together,

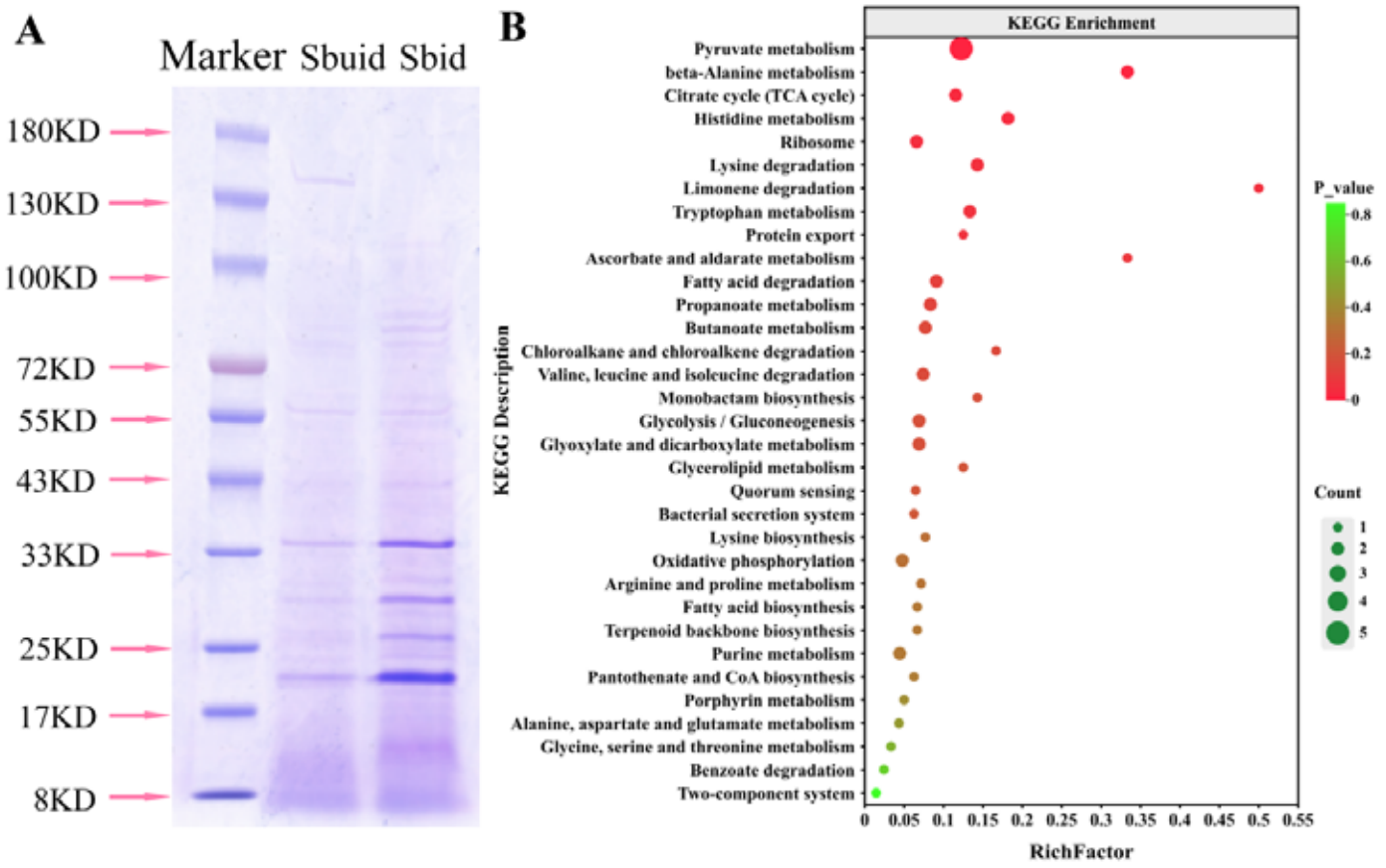

Fig. 3. (A) Polyacrylamide gel electrophoresis (SDS-PAGE) (Sbuid: Sb-uninduced; Sbid: Sb-induced); (B) KEGG enrichment analysis. Statistical analysis of differentially upregulated proteins in the supernatant of *A. johnsonii* induced by Sb compared to the supernatant of non-induced *A. johnsonii*.

XRD and XPS analyses confirmed that the precipitates formed in all supernatants were Sb_2O_3 (Fig. S4B).

Effect of A. johnsonii on Sb uptake and growth of paddy

The biomineralization of heavy metals can reduce their mobility and bioavailability, making it a promising approach for the remediation of Sb-contaminated soils. To evaluate the application of Sb(III) mineralization by *A. johnsonii*, the Sb uptake characteristics and growth responses of rice were systematically invested. First, the properties of the soil used for rice cultivation were characterized. The experimental soil was slightly alkaline (pH 8.0), with a background Sb concentration of 12.53 mg·kg^{-1}, organic

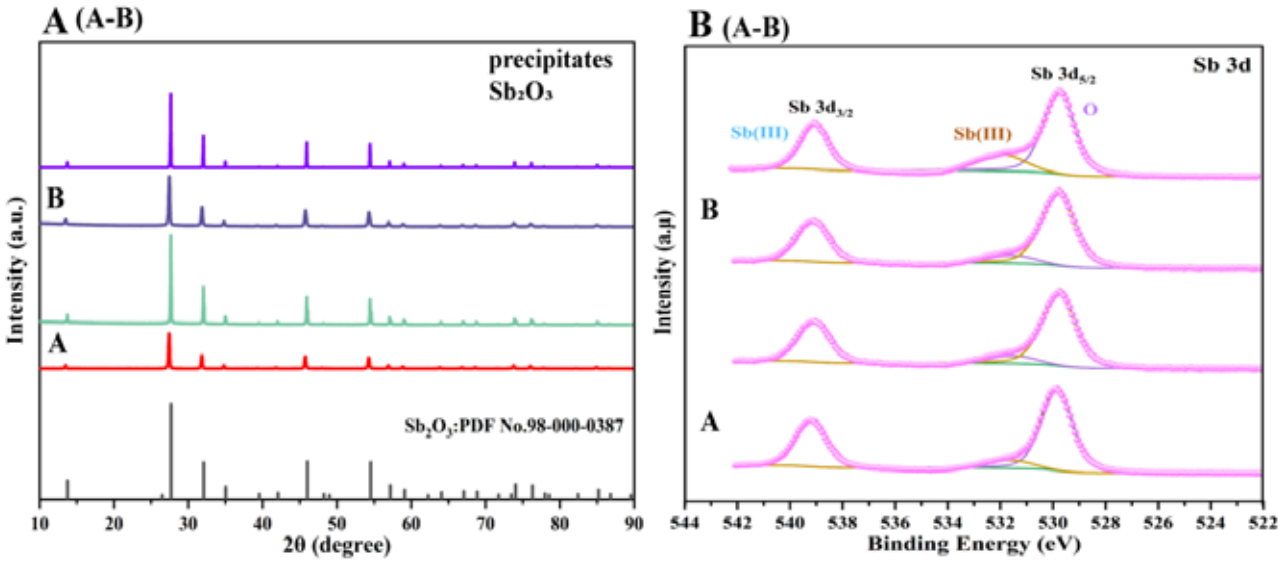

Fig. S4. (A) X-ray diffraction (XRD) corresponded to (A-D) in SEM; (B) X-ray photoelectron spectroscopy (XPS). Referring to figures A and B in figure 4.

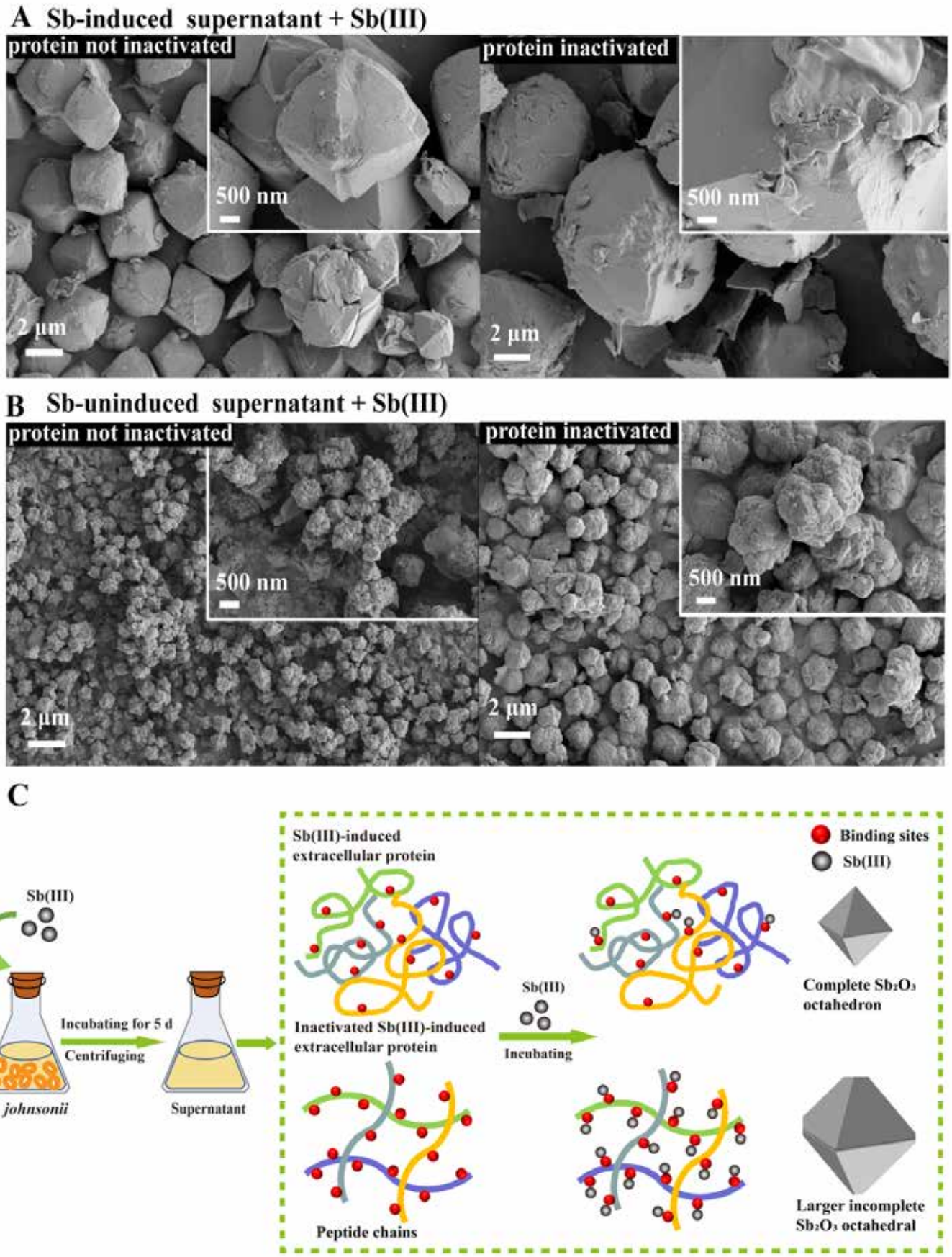

Fig. 4. (A) Sb-induced supernatant with proteins not inactivated and inactivated + 11 mM Sb(III); (B) Sb-uninduced supernatant with proteins not inactivated and inactivated + 11 mM Sb(III); (C) The mechanism diagram illustrates the process by which *A. johnsonii* induces the mineralization of Sb(III). The extracellular proteins secreted by *A. johnsonii* upon induction by Sb(III) can lead to the mineralization of Sb(III), resulting in the formation of complete octahedral-shaped Sb_2O_3 crystals. Inactive extracellular protein peptides expose more binding sites for Sb(III), leading to the formation of larger but incompletely shaped Sb_2O_3 crystals.

Table S1. Significantly up-regulated differential proteins in the Sb-induced supernatant

Description	Pvalue	Gene.Name
autotransporter domain-containing protein	0.031684176	*F946_01272*
citrate synthase	0.049916251	*gltA*
hypothetical protein	0.003506445	*F946_00442*
4-aminobutyrate-2-oxoglutarate transaminase	0.002177729	*puuE*
NADH-quinone oxidoreductase subunit NuoG	0.020090104	*F946_02587*
porin Omp33-36	0.045550828	*omp33-36*
universal stress protein	0.01641211	*nhaX_1*
NADH-quinone oxidoreductase subunit NuoF	0.011240054	*nuoF*
betaine-aldehyde dehydrogenase	0.043301653	*betB*
4-hydroxy-tetrahydrodipicolinate reductase	0.04435586	*dapB*
acetyl-CoA C-acyltransferase	0.033391283	*CFH90_13805*
WxcM-like domain-containing protein	0.0194763	*fdtC*
hydroxyacylglutathione hydrolase	0.034168848	*gloB*
family protein	7.13472E-05	*dsbC_2*
uroporphyrinogen decarboxylase	0.023698752	*hemE*
family metalloprotease	0.002977597	*stcE*
molecular chaperone DnaJ	0.000320915	*dnaJ*
imidazoleglycerol-phosphate dehydratase HisB	0.035758151	*hisB*
50S ribosomal protein L10	0.045389079	*rplJ*
guanine deaminase	0.005090086	*guaD*
acetyl-CoA carboxylase carboxyltransferase subunit alpha	0.009411092	*accA*
cation acetate symporter	0.011755934	*actP_3*
symmetrical bis(5'-nucleosyl)-tetraphosphatase	0.029631893	*DI542_06290*
putative porin	0.001201388	*ACNJC6_01226*
RDD family protein	0.032407055	*ACNJC6_01556*
phosphoenolpyruvate carboxykinase (GTP)	0.000272388	*pckG*
30S ribosomal protein S21	0.00022777	*rpsU*
benzaldehyde dehydrogenase	0.031745954	*N5D11_14455*
Lprotein-export chaperone SecB	0.042692473	*secB*
carbohydrate porin	0.029988448	*DI542_14230*

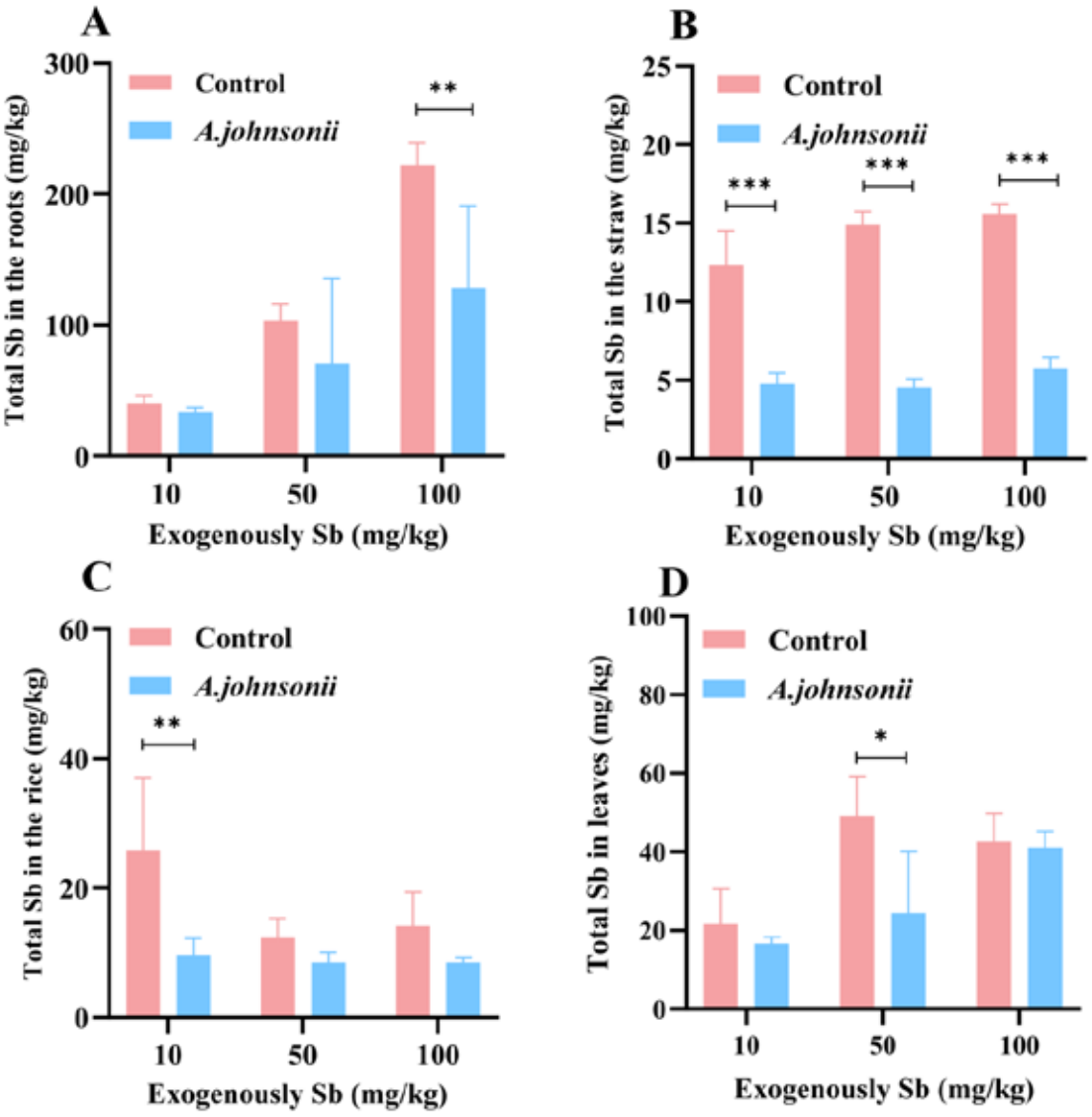

Fig. 5. The application of Sb(III) mineralization by *A. johnsonii* is examined with paddy. (A-D) Sb content in roots, straw, rice, and leaves, respectively. Differences between groups were analyzed using two-way analysis of variance, with $p \leq 0.05$ as significant differences.

In the figure legends, "** " denotes a significant difference ($P < 0.01$), "***" represents a highly significant difference ($P < 0.001$). These symbols are used to show the statistical significance of the differences in total Sb content in different parts of rice, rice production and stem length between the two groups under different exogenous Sb concentrations.

matter content of 8.67 mg·g^{-1}, and elevated levels of plant-available nutrients, including alkaline hydrolyzable nitrogen (324.57 mg·kg^{-1}), available potassium (451.49 mg·kg^{-1}), and available phosphorus (21.13 mg·kg^{-1}). These parameters provided essential environmental context for the growth of both microorganisms and rice. Sb accumulation in rice tissues was subsequently measured, as shown in Fig. 5A-D.

Sb content in rice roots increased with elevated Sb concentrations in both *A. johnsonii*-inoculated and non-inoculated groups (Fig. 5A), reaching 40, 100, and 200 mg·kg^{-1} in non-inoculated groups. However, rice roots inoculated with *A. johnsonii* exhibited lower Sb levels compared to the corresponding non-inoculated controls, and the reduction became more pronounced as Sb concentration increased. In *A. johnsonii*-treated rice, Sb content in the stalk remained stable at approximate 5 mg·kg^{-1} across different Sb(III) concentrations, markedly lower than that in non-inoculated rice (approximately 15 mg·kg^{-1}). Sb content in rice grains and leaves was approximately 15 mg·kg^{-1} and 40 mg·kg^{-1}, respectively. Both tissues showed a decreasing trend in Sb accumulation in *A. johnsonii*-treated paddy compared with untreated paddy under various Sb(III) stress levels, indicating that the highest Sb accumulation occurred in roots. Overall, the distribution of Sb in rice tissues followed the order: roots > leaves > polished grains ≥ stalks (Fig. 5A-D). This uptake pattern suggests that Sb is predominantly sequestered in roots, minimizing its transfer to leaves, stalks, and grains, consistent with previous findings on root barrier effects (Cai, Mi, and Zhang 2016). The effects of *A. johnsonii* on rice growth are shown in Fig. 6. Rice yield in non-inoculated groups declined progressively with increasing Sb concentrations (Fig. 6A), whereas *A. johnsonii*-inoculated plants maintained stable yields across Sb stress levels. Notably, inoculated plants achieved higher yields than non-inoculated controls (Fig. 6B) (Zhang et al. 2024). Plant height showed no

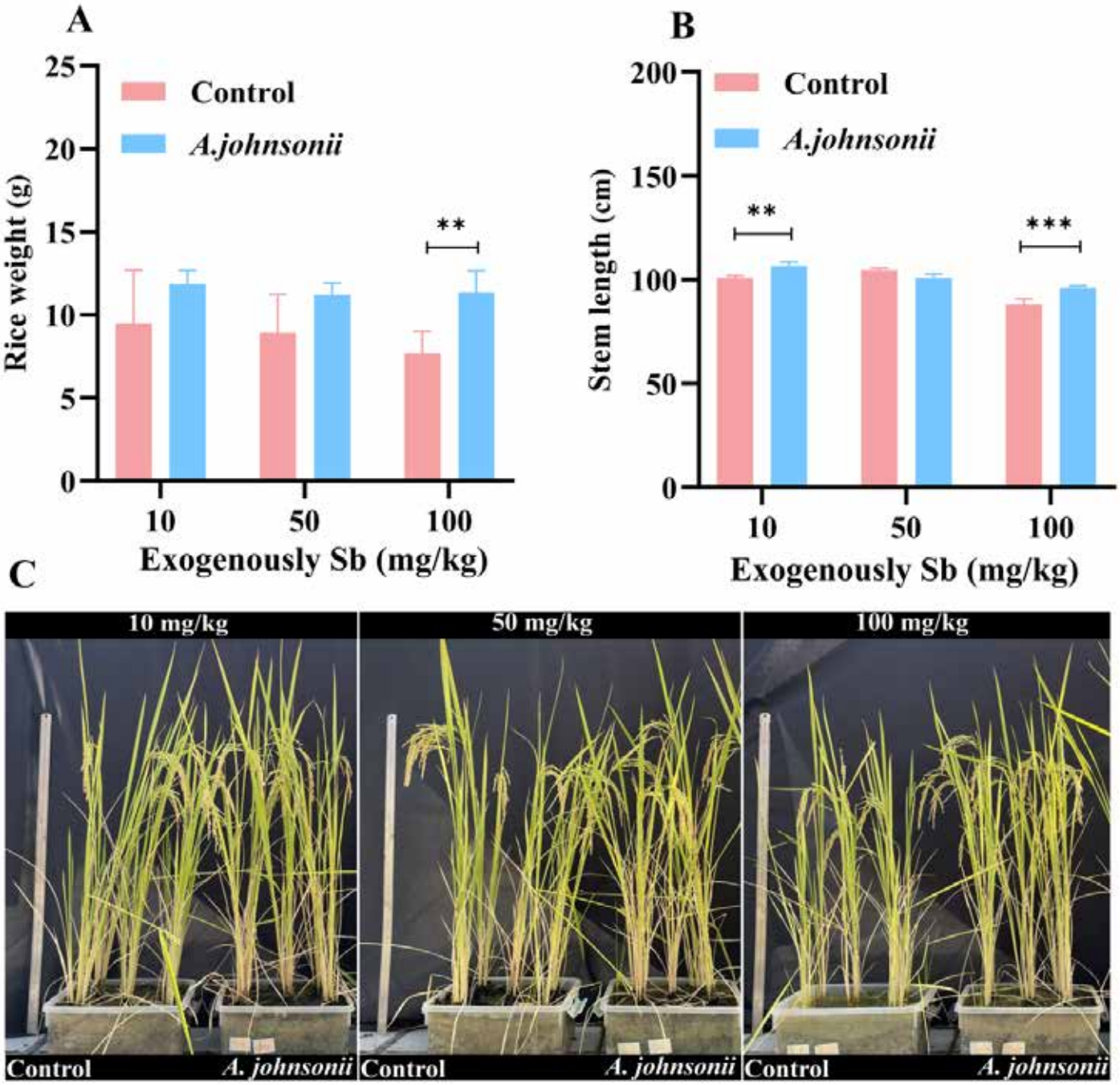

Fig. 6. The application of Sb(III) mineralization by *A. johnsonii* is examined with paddy. (A) yield of rice under different Sb concentrations without and with sterilization; (B) length of stems of rice grown under different antimony concentrations without and with *A. johnsonii*; (C) water growth of rice under different conditions. Differences between groups were analyzed using two-way analysis of variance, with $p \leq 0.05$ as significant differences.
In the figure legends, "** " denotes a significant difference ($P < 0.01$), "***" represents a highly significant difference ($P < 0.001$). These symbols are used to show the statistical significance of the differences in total Sb content in different parts of rice, rice production and stem length between the two groups under different exogenous Sb concentrations.

significant differences between inoculated and non-inoculated groups under 10 and 50 mg·kg^{-1} Sb stress. However, at 100 mg·kg^{-1} Sb, the height of rice inoculated with *A johnsonii* showed a significant increase compared to the control group (Fig. 6C). These results demonstrate that rice possesses a strong Sb accumulation capacity, and that *A. johnsonii* not only reduces Sb uptake in rice but also promotes rice growth under Sb stress, likely through mechanisms involving nutrient activation and inhibition of Sb translocation.

Discussion

Understanding the mechanism of microbially mediated Sb(III) biomineralization is a core prerequisite for overcoming bottlenecks in efficient Sb pollution remediation and for elucidating key links in the Sb biogeochemical cycle. Current research on Sb(III) biomineralization has largely focused on the overall metabolic effects of microorganisms or the role of EPS (Shukla et al. 2019; Yang et al. 2024). However, studies

Table S2. Soil physicochemical properties

Soil pH	Total Sb (mg/kg)	Organic Matter (mg/g)	Hydrolyzable Nitrogen (mg/kg)	Available Potassium (mg/kg)	Available Phosphorus (mg/kg)
8	12.53	8.67	324.57	451.49	21.13

on the molecular mechanisms, key regulatory substances, and morphological control pathways underlying directional Sb(III) biomineralization by specific functional microorganisms remain limited, restricting the precise application of microbial remediation technologies. In this study, we isolated a distinctive strain, *A. johnsonii*, with both alkalinity-producing and directional biomineralization capabilities. More importantly, through a multi-dimensional experimental approach, we systematically revealed, for the first time, the mechanism by which *A. johnsonii* directionally regulates the biomineralization of Sb(III) into Sb_2O_3 via EPS proteins, moving beyond the traditional focus on polysaccharides in EPS. Furthermore, this mechanism was applied in a rice remediation system, achieving the dual functions of "Sb immobilization and plant growth promotion".

Although *A. johnsonii* secretes large amounts of extracellular polysaccharides, experiments confirmed that these polysaccharides alone cannot mediate Sb(III) biomineralization. This study investigated the core mechanism of Sb(III) biomineralization induced by this strain from three dimensions—functional groups, protein expression, and protein structure—and clarified the dominant role of proteins. At the functional group level, proteins, as biomacromolecules rich in functional groups (e.g., C=O, O=C-OH, R-OH, R-NH_2, C-H, S-H), can provide negative charges or lone pairs of electrons (Wang et al. 2018). These groups not only immobilize Sb(III) through electrostatic adsorption but also inhibit the disordered aggregation of crystal nuclei via steric hindrance, thereby regulating crystal growth (Zhou et al. 2010; Cui et al. 2021). 3D-EEM fluorescence spectroscopy revealed that in Sb(III)-induced supernatants, the fluorescence signals of tryptophan (Ex/Em 260/350 nm) and tyrosine derivatives (Ex/Em 275/305 nm) were significantly enhanced, with signal intensity consistent with changes in protein content. These findings confirm that specific protein derivatives play a dominant role in Sb(III) biomineralization.

At the protein expression level, SDS-PAGE showed that bands at 34 kDa and 20 kDa were upregulated under Sb(III) stress. Proteomic analysis identified 30 differentially expressed proteins, 10 of which are involved in metabolic pathways (Table S1). The directional expression of these proteins provides molecular evidence supporting the "protein-dominated biomineralization" hypothesis. Regarding protein structure regulation, protein inactivation experiments (boiling water bath for 1 h) revealed that after protein inactivation, the size of Sb_2O_3 microcrystals increased and the integrity of crystal tops decreased. This indicates that the folded structure of native proteins limits the exposure of Sb(III)-binding sites, whereas linearized peptide chains (after protein denaturation) release additional binding sites, promoting the aggregation of Sb(III) and thus the formation of larger Sb_2O_3 microcrystals (Fig. 4C).

Hydrolyzable nitrogen is an important form of nitrogen directly absorbable by plants from the soil, while potassium and phosphorus are essential nutrients for plant growth. In this study, the soil used for rice cultivation contained a certain amount of Sb but was rich in organic matter, hydrolyzable nitrogen, and readily available potassium, providing sufficient to support healthy rice growth and development (Sadeghi et al. 2023). Exogenously added Sb in this study was in the form of Sb(III), which is the predominant form of Sb under anaerobic conditions. Anaerobic conditions were strictly maintained following the recognized method for rice cultivation (Section 2.7), by keeping a 5 cm saturated water layer on the soil surface throughout the experiment. This flooding approach physically blocks oxygen supply from the air, while rice root respiration and soil microbial metabolism continuously consume residual oxygen. These two factors establish and maintain a stable anaerobic microenvironment in the plow layer soil and rhizosphere, ensuring that Sb exists primarily as Sb(III) in the soil-rice system (Wang et al. 2019). Sb(III) is more readily absorbed by rice than Sb(V), and rice Sb uptake exhibited a significant positive correlation with exogenous Sb concentration (Wang et al. 2019). This is likely due to the presence of Sb(III) transporters in the root exodermis, which facilitate adsorption and transport of Sb(III) into rice roots. Furthermore, the expression of these transporters is concentration-dependent, enhancing Sb uptake as exogenous Sb levels increase. However, Sb absorption and accumulation in rice were tissue-specific, with the majority of Sb deposited in the roots. The limited translocation of Sb from roots to other tissues may be attributed to the absence of efflux transporters in rice roots, resulting in predominant Sb deposition in root tissue.

A. johnsonii can not only directionally convert Sb(III) into octahedral Sb_2O_3 microcrystals, reducing the mobility and bioactivity of Sb(III) and thus enabling survival and proliferation even under 21 mM Sb(III) stress, but also overcome the limitations of traditional microbial remediation by achieving the synergistic effect of "Sb immobilization and growth promotion". This demonstrates the unique potential of *A. johnsonii* for the remediation of Sb-contaminated farmland. Adaptability to environmental factors is key to the efficient functioning of the strain. Regarding pH, *A. johnsonii* possesses an inherent alkalinity-producing ability, stabilizing the culture medium at pH 8.6, which allows it to thrive in the weakly alkaline environmental soil (pH 8). Such near-neutral to slightly alkaline conditions are conducive to bacterial growth (Kushkevych, Dordević, and Vítězová 2019). In terms of organic matter, the experimental soil contained 8.67 $mg \cdot g^{-1}$ organic matter, which not only improves soil structure but also provides a carbon source for the strain, promoting the secretion of Sb(III)-induced extracellular proteins and thereby enhancing biomineralization efficiency (Huo et al. 2024). The growth and proliferation of *A. johnsonii* facilitate the biomineralization

of Sb(III) in soil, reduce Sb accumulation in rice roots, and promote rice growth while stabilizing rice yield under Sb(III) stress. These results show that *A. johnsonii* can efficiently remediate soil Sb(III) pollution while ensuring normal crop growth, achieving the dual functions of "Sb immobilization and growth promotion", and providing a practical approach for the safe utilization of Sb-contaminated farmland.

Conclusion

This study systematically elucidated the mechanism of Sb(III) biomineralization mediated by *A. johnsonii* and demonstrated its potential application for Sb pollution remediation through microbial screening, laboratory cultivation, and paddy soil pot experiments. Regarding the biomineralization mechanism, the efficiency and regulatory effect of *A. johnsonii* on Sb(III) biomineralization are mainly governed by the protein component in EPS. Under Sb(III) induction, extracellular proteins secreted by the strain regulate crystal growth, converting Sb(III) into octahedral Sb_2O_3 microcrystals, with a removal rate of up to 90% for 11 mM Sb(III). In the soil-rice system, rice exhibited strong Sb enrichment, with accumulation following the order of root > leaf > polished grain ≥ stalk. After inoculation with *A. johnsonii*, Sb accumulation in rice roots and other tissues was significantly reduced. The strain also demonstrated excellent environmental adaptability, thriving in the weakly alkaline environmental soil (pH 8) and utilizing soil organic matter to support growth and proliferation. By promoting Sb(III) biomineralization, *A. johnsonii* further enhances rice growth and stabilized yield under Sb(III) stress. Future studies can focus on optimizing the culture conditions of *A. johnsonii* to further enhance Sb(III) biomineralization efficiency, thereby facilitating its field application in Sb-contaminated farmlands. This research provides a promising strategy for microbial remediation of farmland Sb pollution, achieving both soil Sb control and safe crop production. Further exploration of the coupling effect of this strain with other remediation technologies, as well as the molecular regulatory mechanisms of key proteins involved in Sb(III) biomineralization, will provide more comprehensive technical and theoretical support for Sb pollution management.

Declaration of Competing Interest

The authors declare that they have no known competing financial interests or personal relationships that could have appeared to influence the work reported in this paper.

Acknowledgements

This work was supported by the National Natural Science Foundation of China (32101045), the Introducing Talent in Guizhou University 2020 (17).

References

Cai, Yongbing, Yuting Mi, and Hua Zhang. (2016). Kinetic modeling of antimony(III) oxidation and sorption in soils. *Journal of Hazardous Materials*, 316, pp. 102-109. DOI:10.1016/j.jhazmat.2016.05.027.

Chen, Yin, Wenjun Mao, Hongwen Tao, Weiming Zhu, Xiaohui Qi, Yanli Chen, Hongyan Li, Chunqi Zhao, Yupin Yang, Yujiao Hou, Chunyan Wang, and Na Li. (2011). Structural characterization and antioxidant properties of an exopolysaccharide produced by the mangrove endophytic fungus Aspergillus sp. Y16. *Bioresource Technology*, 102, 17, pp. 8179-8184. DOI:10.1016/j.biortech.2011.06.048.

Chen, Zhao, Bingqing Xia, Yang Yang, Shiwen Hu, Kuan Cheng, Pengfei Cheng, Shan Wang, Guojun Chen, Qi Wang, Haibo Dong, Chao Guo, Yating Chen, and Tongxu Liu. (2024). Evaluating the influence of alternating flooding and drainage on antimony speciation and translocation in a soil-rice system. *Science of The Total Environment*, 957, pp. 177721. DOI:10.1016/j.scitotenv.2024.177721.

Cui, Linlin, Ling Fan, Zhanfei Li, Junjun Wang, Ran Chen, Yejuan Zhang, Jinju Cheng, Xueling Wu, Jiaokun Li, Huaqun Yin, Weiming Zeng, and Li Shen. (2021). Characterization of extracellular polymeric substances from Synechocystis sp. PCC6803 under Cd (II), Pb (II) and Cr (VI) stress. *Journal of Environmental Chemical Engineering*, 9, 4, pp. 105347. DOI:10.1016/j.jece.2021.105347.

Devi, Rajni, Biswaranjan Behera, Md Basit Raza, Vikas Mangal, Muhammad Ahsan Altaf, Ravinder Kumar, Awadhesh Kumar, Rahul Kumar Tiwari, Milan Kumar Lal, and Brajesh Singh. (2021). An Insight into Microbes Mediated Heavy Metal Detoxification in Plants: a Review. *Journal of Soil Science and Plant Nutrition*, 22, 1, pp. 914-936. DOI:10.1007/s42729-021-00702-x.

Dong, Hailiang, Liuqin Huang, Linduo Zhao, Qiang Zeng, Xiaolei Liu, Yizhi Sheng, Liang Shi, Geng Wu, Hongchen Jiang, Fangru Li, Li Zhang, Dongyi Guo, Gaoyuan Li, Weiguo Hou, and Hongyu Chen. (2022). A critical review of mineral–microbe interaction and co-evolution: mechanisms and applications. *National Science Review*, 9, 10, pp. 10. DOI:10.1093/nsr/nwac128.

Gaur, Vivek Kumar, Poonam Sharma, Prachi Gaur, Sunita Varjani, Huu Hao Ngo, Wenshan Guo, Preeti Chaturvedi, and Reeta Rani Singhania. (2021). Sustainable mitigation of heavy metals from effluents: Toxicity and fate with recent technological advancements. *Bioengineered*, 12, 1, pp. 7297-7313. DOI:10.1080/21655979.2021.1978616.

He, Jun, Yubin Hong, Yihang Zhao, Xinyu Hong, Xinye Cheng, Yongjian Xie, Qingqing Xiao, Wanrou Liu, Lihua Dong, Li'an Hou, and Diyun Chen. (2025). Fate and behavior of uranium biomineralization by the native Burkholderia sp. S1 isolated from tailing areas. *Journal of Environmental Chemical Engineering*, 13, 3, pp. 116602. DOI:10.1016/j.jece.2025.116602.

He, Si-Xue, You-Jing Peng, Jia-Yi Chen, Chen-Jing Liu, Yue Cao, Wei Li, and Lena Q. Ma. (2023). Antimony uptake and speciation, and associated mechanisms in two As-hyperaccumulators Pteris vittata and Pteris cretica. *Journal of Hazardous Materials*, 455, pp. 131607. DOI:10.1016/j.jhazmat.2023.131607.

He, Yizhou, Yang Yang, Wenting Chi, Shiwen Hu, Guojun Chen, Qi Wang, Kuan Cheng, Chao Guo, Tongxu Liu, and Bingqing Xia. (2024). Biogeochemical cycling in paddy soils controls antimony transformation: Roles of iron (oxyhydr)oxides, organic matter and sulfate. *Journal of Hazardous Materials*, 464, pp. 32979. DOI:10.1016/j.jhazmat.2023.132979.

Huo, Xiaokang, Yumeng Zhou, Ning Zhu, Xiaopeng Guo, Wen Luo, Yan Zhuang, Feifan Leng, and Yonggang Wang. (2024). Soil Organic Matter and Total Nitrogen Reshaped Root-Associated

Bacteria Community and Synergistic Change the Stress Resistance of Codonopsis pilosula. *Molecular Biotechnology*, 67, pp. 2545-2561. DOI:10.1007/s12033-024-01217-3.

Jabłońska-Czapla et al. (2022). Antimony speciation in soils in areas subjected to industrial anthropopressure. *Archives of Environmental Protection*, 42, pp. 5. DOI:10.24425/aep.2022.140765.

Jabłońska-Czapla, Magdalena, Marzena Rachwał, Katarzyna Grygoyć, and Małgorzata Wawer-Liszka. (2024). Application of soil magnetometry and geochemical methods to investigate soil contamination with antimony. *Environmental Geochemistry and Health*, 46, 8, pp. 287. DOI:10.1007/s10653-024-02086-0.

Jabłońska-Czapla, Magdalena, Sebastian Szopa, Piotr Zerzucha, Aleksandra Łyko, and Rajmund Michalski. (2015). Chemometric and environmental assessment of arsenic, antimony, and chromium speciation form occurrence in a water reservoir subjected to thermal anthropopressure. *Environmental Science and Pollution Research*, 22, 20, pp. 15731-15744. DOI:10.1007/s11356-015-4769-z.

Kondakindi, Venkateswar Reddy, Ranjit Pabbati, Priyanka Erukulla, Naga Raju Maddela, and Ram Prasad. (2024). Bioremediation of heavy metals-contaminated sites by microbial extracellular polymeric substances – A critical view. *Environmental Chemistry and Ecotoxicology*, 6, pp. 408-421. DOI:10.1016/j.enceco.2024.05.002.

Kushkevych, Ivan, Dani Dordević, and Monika Vítězová. (2019). Analysis of pH dose-dependent growth of sulfate-reducing bacteria. *Open Medicine*, 14, 1, pp. 66-74. DOI:10.1515/med-2019-0010.

Long, Jiumei, Di Tan, Sihan Deng, and Ming Lei. (2018). Uptake and accumulation of potentially toxic elements in colonized plant species around the world's largest antimony mine area, China. *Environmental Geochemistry and Health*, 40, 6, pp. 2383-2394. DOI:10.1007/s10653-018-0104-1.

Sadeghi, Sara, Billi Jean Petermann, Joshua J. Steffan, Eric C. Brevik, and Csongor Gedeon. (2023). Predicting microbial responses to changes in soil physical and chemical properties under different land management. *Applied Soil Ecology*, 188, pp. 104878. DOI:10.1016/j.apsoil.2023.104878.

Shukla, Arpit, Krina Mehta, Jignesh Parmar, Jaimin Pandya, and Meenu Saraf. (2019). Depicting the exemplary knowledge of microbial exopolysaccharides in a nutshell. *European Polymer Journal*, 119, pp. 298-310. DOI:10.1016/j.eurpolymj.2019.07.044.

Si, Meiyan, Yuntao Zhang, Hai Jin, Yongliang Long, Tao Nie, Wei Feng, Qingsong Li, Yichao Lin, Xiaoqian Xu, and Chunhua Wang. (2024). Research progress on acid mine drainage treatment based on CiteSpace analysis. *Archives of Environmental Protection*, 50, 4, pp. 104-115. DOI:10.24425/aep.2024.152900.

Wang, Bin-Bin, Xue-Ting Liu, Jian-Meng Chen, Dang-Cong Peng, and Feng He. (2018). Composition and functional group characterization of extracellular polymeric substances (EPS) in activated sludge: the impacts of polymerization degree of proteinaceous substrates. *Water Research*, 129, pp. 133-142. DOI:10.1016/j.watres.2017.11.008.

Wang, Xiangqin, Fangbai Li, Chaolei Yuan, Bin Li, Tongxu Liu, Chengshuai Liu, Yanhong Du, and Chuanping Liu. (2019). The translocation of antimony in soil-rice system with comparisons to arsenic: Alleviation of their accumulation in rice by simultaneous use of Fe(II) and NO^{3-}. *Science of The Total Environment*, 650, pp. 633-641. DOI:10.1016/j.scitotenv.2018.09.054.

Wu, Tongliang, Xiaodan Cui, Syed Tahir Ata-Ul-Karim, Peixin Cui, Cun Liu, Tingting Fan, Qian Sun, Hua Gong, Dongmei Zhou, and Yujun Wang. (2022). The impact of alternate wetting and drying and continuous flooding on antimony speciation and uptake in a soil-rice system. *Chemosphere*, 297, pp. 134147. DOI:10.1016/j.chemosphere.2022.134147.

Yang, Linping, Aijiang Yang, Liyan Song, Wen Cui, Wanping Bian, Aping Niu, Peng Xu, Shouyang He, Shixue Mei, and Xianrong Shi. (2024). Formation of Sb_2O_3 microcrystals by Rhodotorula mucilaginosa. *Journal of Hazardous Materials*, 469, pp. 134082. DOI:10.1016/j.jhazmat.2024.134082.

Yu, Huang, Xizhe Yan, Wanlin Weng, Sihan Xu, Guizhi Xu, Tianyuan Gu, Xiaotong Guan, Shengwei Liu, Pubo Chen, Yongjie Wu, Fanshu Xiao, Cheng Wang, Longfei Shu, Bo Wu, Dongru Qiu, Zhili He, and Qingyun Yan. (2022). Extracellular proteins of Desulfovibrio vulgaris as adsorbents and redox shuttles promote biomineralization of antimony. *Journal of Hazardous Materials*, 426, pp. 127795. DOI:10.1016/j.jhazmat.2021.127795.

Yuan, Shi-Jie, Min Sun, Guo-Ping Sheng, Yin Li, Wen-Wei Li, Ri-Sheng Yao, and Han-Qing Yu. (2011). Identification of key constituents and structure of the extracellular polymeric substances excreted by Bacillus megaterium TF10 for their flocculation capacity. *Environmental science & technology*, 45, 3, pp. 1152-1157. DOI:10.1021/es1030905.

Zhang, Kejing, Dawei Zhang, Xiao Li, and Yingwen Xue. (2022). Biomineralization of lead in wastewater: Bacterial reutilization and metal recovery. *Journal of Hazardous Materials*, 421, pp. 126765. DOI:10.1016/j.jhazmat.2021.126765.

Zhang, Liping, Qianqian Yang, Shiliang Wang, Wanting Li, Shaoqing Jiang, and Yan Liu. (2017). Influence of silicon treatment on antimony uptake and translocation in rice genotypes with different radial oxygen loss. *Ecotoxicology and Environmental Safety*, 144, pp. 572-577. DOI:10.1016/j.ecoenv.2017.06.076.

Zhang, Yu, Si-Yu Zhao, Ruo-Han Zhang, B. Larry Li, Yu-Ying Li, Hui Han, Peng-Fei Duan, and Zhao-Jin Chen. (2024). Screening of plant growth-promoting rhizobacteria helps alleviate the joint toxicity of PVC+Cd pollution in sorghum plants. *Environmental Pollution*, 355, pp. 124201. DOI:10.1016/j.envpol.2024.124201.

Zhou, Gen-Tao, Ye-Bin Guan, Qi-Zhi Yao, and Sheng-Quan Fu. (2010). Biomimetic mineralization of prismatic calcite mesocrystals: Relevance to biomineralization. *Chemical Geology*, 279, 3-4, pp. 63-72. DOI:10.1016/j.chemgeo.2010.08.020.